Two-Dimensional Versus Three-Dimensional Symmetric Lifting Motion Prediction Models: A Case Study

Rahid Zaman
School of Mechanical and Aerospace Engineering,
Oklahoma State University,
Stillwater, OK 74078
e-mail: grana@okstate.edu

Yujiang Xiang[1]
School of Mechanical and Aerospace Engineering,
Oklahoma State University,
Stillwater, OK 74078
e-mail: yujiang.xiang@okstate.edu

Jazmin Cruz
Human-Centric Design Research Lab,
Department of Mechanical Engineering,
Texas Tech University,
Lubbock, TX 79409
e-mail: jazmin.aguilar@ttu.edu

James Yang
Human-Centric Design Research Lab,
Department of Mechanical Engineering,
Texas Tech University,
Lubbock, TX 79409
e-mail: james.yang@ttu.edu

Symmetric lifting is a common manual material handling strategy in daily life and is the main cause of low back pain. In the literature, symmetric lifting is mainly simulated by using two-dimensional (2D) models because of their simplicity and low computational cost. In practice, however, symmetric lifting can generate asymmetric kinetics especially when the lifting weight is heavy and symmetric lifting based on 2D models misses this important asymmetric kinetics information. Therefore, three-dimensional (3D) models are necessary for symmetric lifting simulation to capture asymmetric kinetics. The purpose of this single-subject case study is to compare the optimization formulations and simulation results for symmetric lifting by using 2D and 3D human models and to identify their pros and cons. In this case study, a 10-degrees-of-freedom (DOFs) 2D skeletal model and a 40-DOFs 3D skeletal model are employed to predict the symmetric maximum weight lifting motion, respectively. The lifting problem is formulated as a multi-objective optimization (MOO) problem to minimize the dynamic effort and maximize the box weight. An inverse dynamic optimization approach is used to determine the optimal lifting motion and the maximum lifting weight considering dynamic joint strength. Lab experiments are carried out to validate the predicted motions. The predicted lifting motion, ground reaction forces (GRFs), and maximum box weight from the 2D and 3D human models for Subject #8 are compared with the experimental data. Recommendations are given. [DOI: 10.1115/1.4049217]

Keywords: symmetric lifting, two-dimensional model, three-dimensional model, maximum weight lifting, dynamic joint strength, inverse dynamic optimization, computer-aided engineering, physics-based simulations

1 Introduction

Despite the advancement in robotics and automation fields, manual material handling (MMH)-related injuries like hyperextension and occupational hazards are the most common cause of disability [1]. Low back pain from hyperextension is the leading cause for visits to orthopedic surgeons and neurosurgeons and the second common cause for visits to physicians [2,3]. Symmetric lifting is one of the most common causes of musculoskeletal disorders (MSDs) like low back pain [4,5]. Therefore, it is necessary to identify the maximum lifting weight for a person as well as the reasons behind lifting work-related injuries. In practice, it is difficult to find the best lifting motion and true maximum lifting weight through laboratory experiments as it is risky for the participants [6–8]. An optimization-based biomechanical model can assist in finding the best lifting motion as well as the maximum lifting weight.

Over the past decades, many researchers have been working on human biomechanical modeling. However, only a few researchers have worked on lifting motion prediction using 3D human models [9–11]. Many researchers worked on the 2D human models [12–20]. For example, based on the National Institute of Occupational Safety and Health (NIOSH) lifting equation, a static and 2D biomechanical model was proposed to estimate the strength needed for a specific MMH task [12]. In another study, a five-link sagittal model was used to predict the optimum lifting motion using forward dynamic optimization [13]. Another five-link 2D model was introduced to predict the lifting motion based on the static joint strength [14]. The dynamic joint strength is a function of joint angle and angular velocity [21–23] and is more accurate than the static joint strength. In a study by Gündogdu et al. [16], a 2D dynamic-joint-strength-based model was presented to predict the optimal lifting motion using a generic algorithm. Another 2D human model was proposed to predict the symmetric maximum weight lifting motion based on the dynamic joint strength [6,7]. Sreenivasa et al. [20] used a 12-DOF 2D model to study the influence of hip and lumbar flexibility during lifting motion considering the dynamic joint strength.

An optimization-based approach is an effective way to solve a redundant system. As a multi-link human model is a highly redundant system, an optimization-based approach is a preferred tool to find the optimal lifting motion. However, for optimization-based approaches, choosing the objective functions plays a vital role in predicting the lifting motion accurately. A 2D model was developed based on multi-objective optimization (MOO) to predict the lifting motion [6]. The MOO approach results in an 18.9% reduction in the overall joint angle root-mean-square (RMS) error when compared to the single objective optimization-based lifting motion prediction [18]. However, 2D models do not give the total scenario of a lifting motion, as they do not consider lifting unevenly distributed weight on two sides of a sagittal plane of a human body. A 3D model can give more insight into the lifting motion [10,11,24]. A 3D skeletal model was used with four objective functions including spine compression and shear stress to analyze the lifting motion [10]. MOO was also incorporated in a 3D model to predict the lifting motion more accurately [11,24].

In the present work, symmetric maximum weight lifting is simulated by using 2D and 3D human models, respectively. The optimization formulation between the two models is compared. In addition, the simulation results for the maximum box weight, the corresponding optimal joint angle, and GRF profiles for Subject #8 are compared against the experimental data. The pros and cons of 2D and 3D human models for symmetric lifting are summarized. It is concluded that the 3D model can predict more accurate kinetics for symmetric lifting, and the 2D model is a simplified model to

[1]Corresponding author.

Manuscript received June 19, 2020; final manuscript received November 21, 2020; published online February 11, 2021. Assoc. Editor: Caterina Rizzi.

capture the major biomechanics features. In addition, the 2D model is computationally more efficient than the 3D human model.

2 Methods

2.1 Two-Dimensional and Three-Dimensional Human Models. The 2D model has $n = 10$ degrees-of-freedom (DOFs): three global DOFs (q_1, q_2, and q_3) and seven human body joints (q_4, …, q_{10}) as shown in Fig. 1. The global DOFs include two translations and one rotation which move the pelvis to the current position in inertial Cartesian coordinates, while each human body joint is represented by a single rotation in 2D. The total DOFs are defined as $\mathbf{q} = [q_1, \ldots, q_{10}]^T$. Besides the spine joint, since the model is symmetric in the sagittal plane, only one set of shoulder (q_5), elbow (q_6), hip (q_7), knee (q_8), ankle (q_9), and metatarsophalangeal (q_{10}) joints are modeled. In addition, for these symmetric joints, the values of joint strength, link mass, and moment of inertia are doubled.

The 3D skeletal model consists of 40 DOFs, which are expressed as $\mathbf{q} = [z_1\ z_2\ z_3 \ldots .. z_{40}]$. The model consists of one virtual branch and five physical branches. The virtual branch includes three rotational DOFs and three translational DOFs, which allows the model to move in the global space. On the other hand, physical branches are the spine, right arm, left arm, right leg, and left leg. There are six DOFs for the spine, seven DOFs for each arm, and seven DOFs for each leg. Each arm consists of three segments: upper arm, forearm, and hand. Each leg consists of four segments: thigh, shank, rear foot, and forefoot.

The anthropometric data of the models are generated in Visual 3D® (C-Motion, Inc., Germantown, MD) software using experimentally measured height, weight, and stature data. The dynamic joint strength of the models is retrieved from the symmetric maximum weight lifting experiment [23]. The kinematic chains are connected using well-developed Denavit–Hartenberg (DH) representations [25].

2.2 Equations of Motion. The general equations of motion of these biomechanical models are based on the recursive Lagrangian formulation and can be expressed in matrix form, which contains forward recursive kinematics and backward recursive dynamics [26].

Forward recursive kinematics:

$$\mathbf{A}_i = \mathbf{A}_{i-1}\mathbf{T}_i \tag{1}$$

$$\mathbf{B}_i = \dot{\mathbf{A}}_i = \mathbf{B}_{i-1}\mathbf{T}_i + \mathbf{A}_{i-1}\frac{\partial \mathbf{T}_i}{\partial q_i}\dot{q}_i \tag{2}$$

$$\mathbf{C}_i = \dot{\mathbf{B}}_i = \mathbf{C}_{i-1}\mathbf{T}_i + 2\mathbf{B}_{i-1}\frac{\partial \mathbf{T}_i}{\partial q_i}\dot{q}_i + \mathbf{A}_{i-1}\frac{\partial^2 \mathbf{T}_i}{\partial q_i^2}\dot{q}_i^2 + \mathbf{A}_{i-1}\frac{\partial \mathbf{T}_i}{\partial q_i}\ddot{q}_i \tag{3}$$

where q_i is the joint angle variable, $\mathbf{T}_i$ is the 4×4 Denavit–Hartenberg link transformation matrix from the $(i-1)$th link frame to the ith link frame; $\mathbf{A}_i$, $\mathbf{B}_i$, and $\mathbf{C}_i$ are the global recursive kinematics position, velocity, and acceleration matrices, respectively, and $\mathbf{A}_0 = [\mathbf{I}]$, $\mathbf{B}_0 = \mathbf{C}_0 = [0]$.

Backward recursive dynamics:

Each joint torque is defined by Eq. (4)

$$\tau_i = \mathrm{tr}\left(\frac{\partial \mathbf{A}_i}{\partial q_i}\mathbf{D}_i\right) - \mathbf{g}^T\frac{\partial \mathbf{A}_i}{\partial q_i}\mathbf{E}_i - \mathbf{f}_k^T\frac{\partial \mathbf{A}_i}{\partial q_i}\mathbf{F}_i - \mathbf{G}_i^T\mathbf{A}_{i-1}\mathbf{z}_0 \tag{4}$$

$$\mathbf{D}_i = \mathbf{I}_i\mathbf{C}_i^T + \mathbf{T}_{i+1}\mathbf{D}_{i+1} \tag{5}$$

$$\mathbf{E}_i = m_i\mathbf{r}_i + \mathbf{T}_{i+1}\mathbf{E}_{i+1} \tag{6}$$

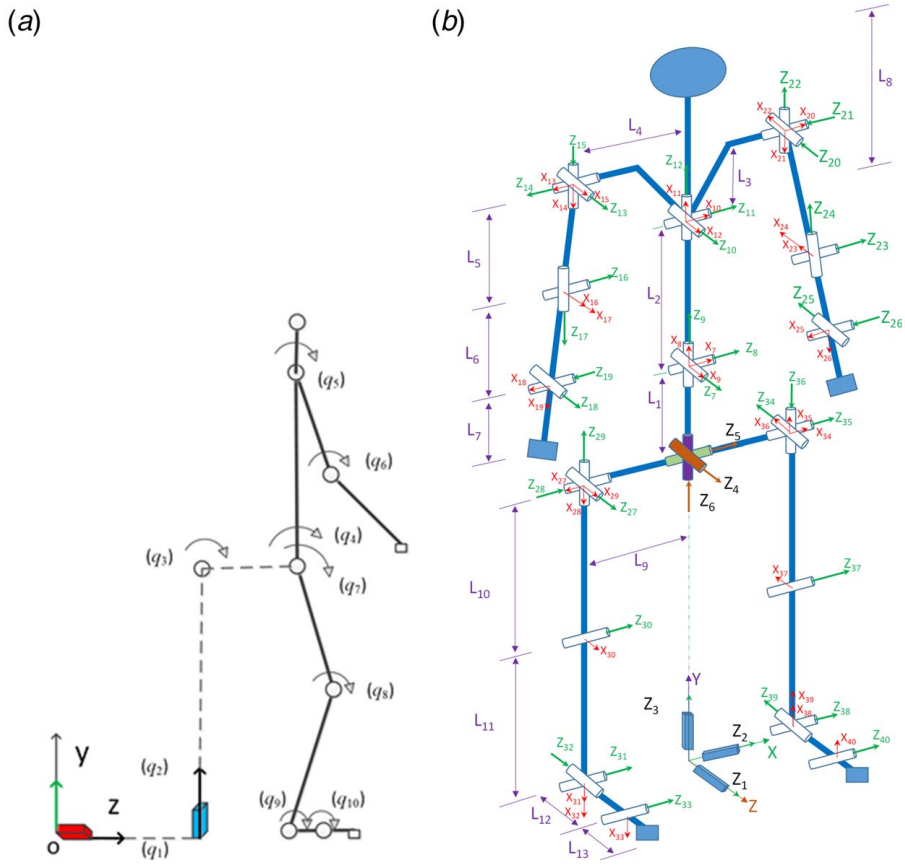

Fig. 1 Human models: (*a*) 10 DOF 2D model and (*b*) 40 DOF 3D model

$$\mathbf{F}_i = \mathbf{r}_k \delta_{ik} + \mathbf{T}_{i+1}\mathbf{F}_{i+1} \tag{7}$$

$$\mathbf{G}_i = \mathbf{h}_k \delta_{ik} + \mathbf{G}_{i+1} \tag{8}$$

where tr(·) is the trace of a matrix, $\mathbf{I}_i$ is the inertia matrix for link i, $\mathbf{D}_i$ is the recursive inertia and Coriolis matrix, $\mathbf{E}_i$ is the recursive vector for gravity torque calculation, $\mathbf{F}_i$ is the recursive vector for external force torque calculation, $\mathbf{G}_i$ is the recursive vector for external moment torque calculation, $\mathbf{g}$ is the gravity vector, m_i is the mass of link i, $\mathbf{r}_i$ is the center of mass of link i, $\mathbf{f}_k$ is the external force applied on link k, $\mathbf{r}_k$ is the position of the external force in the local frame k, $\mathbf{h}_k$ is the external moment applied on link k, $\mathbf{z}_0 = \begin{bmatrix} 0 & 0 & 1 & 0 \end{bmatrix}^T$ is for a revolute joint, $\mathbf{z}_0 = \begin{bmatrix} 0 & 0 & 0 & 0 \end{bmatrix}^T$ is for a prismatic joint, δ_{ik} is Kronecker delta, and the starting conditions are $\mathbf{D}_{n+1} = [0]$, $\mathbf{E}_{n+1} = \mathbf{F}_{n+1} = \mathbf{G}_{n+1} = [0]$. For 2D model, $\mathbf{f}_k = \begin{bmatrix} 0 & f_{ky} & f_{kz} & 0 \end{bmatrix}^T$ and $\mathbf{h}_k = \begin{bmatrix} h_x & 0 & 0 & 0 \end{bmatrix}^T$, whereas for 3D model $\mathbf{f}_k = \begin{bmatrix} f_{kx} & f_{ky} & f_{kz} & 0 \end{bmatrix}^T$ and $\mathbf{h}_k = \begin{bmatrix} h_x & h_y & h_z & 0 \end{bmatrix}^T$.

2.3 Optimization Formulation. For the optimization problem, the time domain is discretized by using cubic B-spline functions. With this representation, the control points ($\mathbf{P}$) become the optimization variables. In this study, the box weight (W) and total time duration (T) are also treated as design variables. Then, the joint angular velocity ($\dot{\mathbf{q}}$) and acceleration ($\ddot{\mathbf{q}}$) can be obtained from the first- and second-time derivatives of the B-spline discretization of the joint angle profile, respectively. Therefore, all joint state variables ($\mathbf{q}$, $\dot{\mathbf{q}}$, $\ddot{\mathbf{q}}$) are functions of B-spline control points ($\mathbf{P}$) and total time duration T. In addition, the joint torque $\boldsymbol{\tau}(\mathbf{x})$ is computed by plugging the joint state variables and box weight (external load) directly into equations of motion Eq. (4), and this is the inverse dynamics procedure. The lifting task is formulated as a general nonlinear programming (NLP) problem:

Find $\mathbf{x} = \begin{bmatrix} \mathbf{P}^T & W & T \end{bmatrix}^T$

Minimize the dynamic effort and maximize the lifting weight. Finally, the combined objective function is defined as [6]

$$J = w_1 \mathrm{N}\left[\int_0^T \sum_{i=j}^{n} \left(\frac{\tau_i(\mathbf{x}, t)}{\tau_i^U - \tau_i^L}\right)^2 dt\right] - w_2 \mathrm{N}[\log(W + 10)] \tag{9}$$

where N[·] is the normalization function, n is the number of DOFs, j is the first physical joint index: for 2D model $j = 4$ and for 3D model $j = 7$, τ_i^L and τ_i^U are the ith lower and upper dynamic joint torque limits, respectively; w_1 and w_2 are weighting coefficients for the two normalized objective functions where $w_1 = 0.15$ and $w_2 = 0.85$ [6].

Table 1 Constraints for 2D and 3D symmetric lifting optimization formulation

	2D model	3D model
Time-dependent constraints		
(1) Joint angle limit	×	×
(2) Dynamic joint torque limits	×	×
(3) Foot-contacting position	×	×
(4) Dynamic balance	×	×
(5) Box collision avoidance	×	×
(6) Hand distance constraint		×
(7) Box ground parallel constraint		×
(8) Weight difference on hands		×
(9) Kinematic symmetry for lifting		×
Time-independent constraints		
(10) Initial and final box locations	×	×
(11) Initial and final static conditions	×	×
(12) Initial, mid-time, final joint angles	×	×
(13) Initial, intermediate, final GRFs		×

The 2D and 3D symmetric lifting motion optimizations share some common time-dependent constraints including (1) joint angle limits, (2) dynamic joint torque limits, (3) foot-contacting position constraint, (4) dynamic balance constraint, and (5) box collision avoidance constraint (Table 1). The details of these constraints are referred in the study by Xiang et al. [6]. There are additional constraints for the 3D model as detailed below.

2.3.1 Additional Time-Dependent Constraints for Three-Dimensional Lifting. (6) For grasping the box, hand distance constraint is imposed to keep the distance between the two wrists in 3D space equal to the box width and is expressed as

$$\| \mathbf{p}_{right\_hand}(\mathbf{x}, t) - \mathbf{p}_{left\_hand}(\mathbf{x}, t) \|_2 = wid \tag{10}$$

where $\mathbf{p}_{right\_hand}$ and $\mathbf{p}_{left\_hand}$ are the right- and left-hand locations, respectively, and wid is the width of the box.

(7) The box and ground parallel constraint is necessary to keep the box parallel to the ground and is imposed by keeping both hand height at the same level in 3D space.

$$h_{right\_hand}(\mathbf{x}, t) = h_{left\_hand}(\mathbf{x}, t) \tag{11}$$

where h_{right_hand} and h_{left_hand} are the right- and left-hand heights, respectively.

(8) The subject is a righthand dominated person. The load on right hand could be larger than the load on left hand, and the range is within 20 N.

$$0 \le W_{right\_hand}(\mathbf{x}, t) - W_{left_{hand}}(\mathbf{x}, t) \le 20 \tag{12}$$

(9) Joint angle symmetric constraints with [−0.1, 0.1] radian limits are applied during the lifting motion as the experimental lifting motion has almost symmetric kinematics.

2.3.2 Additional Time-Independent Constraints for Three-Dimensional Lifting. (13) Initial, intermediate, and final vertical ground reaction forces (GRFs) constraints are imposed using experimental data

$$|GRF_{left}(\mathbf{x}, t) - GRF_{left}^E(t)| \le 40, \quad t = 0, \ \frac{T}{3}, \ \frac{T}{2}, \ \frac{2T}{3}, \ T \tag{13}$$

$$|GRF_{right}(\mathbf{x}, t) - GRF_{right}^E(t)| \le 40, \quad t = 0, \ \frac{T}{3}, \ \frac{T}{2}, \ \frac{2T}{3}, \ T \tag{14}$$

where GRF_{left}^E and GRF_{right}^E are the experimental vertical ground reaction force for the left foot and right foot, respectively.

The optimal lifting motion is solved using the sequential quadratic programming (SQP)-based Sparse Nonlinear OPTimizer (SNOPT) [27].

2.4 Experimental Data Collection. To evaluate the accuracy of both models, experimental data of Subject #8 for symmetric

Table 2 Anthropometry data of Subject #8

Subject #	8
Age (years old)	28
Weight (kg)	83.73
Height (m)	1.82
Leg length (m)	0.8128
Knee width (m)	0.11
Ankle width (m)	0.068
Shoulder offset (m)	0.053
Elbow width (m)	0.09
Wrist width (m)	0.059
Hand thickness (m)	0.033
InterASIS distance (m)	0.245

Fig. 2 Symmetric box lifting experiment

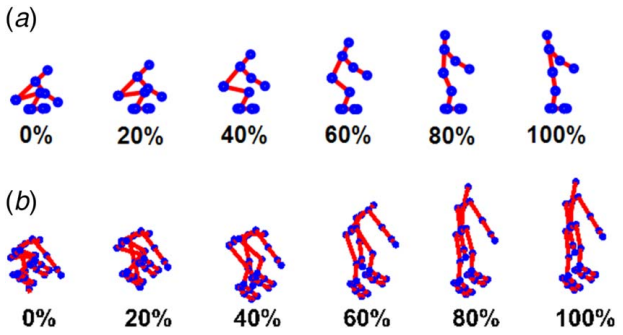

Fig. 3 Snapshots of the predicted symmetric lifting motions: (*a*) 2D model and (*b*) 3D model

weight lifting were collected and compared with the simulation data. Subject #8's anthropometric data are listed in Table 2. The participant signed an informed consent form, and the experimental protocol was approved by the Texas Tech University Institutional Review Board.

Motion data were collected from 42 reflective markers (9 mm, spherical) using a 5-camera Vicon® system (Vicon Motion Systems, Ltd., Oxford, UK) at 100 Hz. GRF data were collected using two Kistler® force plates (Kistler, Winterthur, Switzerland) at 2000Hz.

The maximum lifting weight determined in the experiment is the safe maximum lifting weight, rather than the true maximum weight a subject can lift. To determine the maximum lifting weight, the participant was instructed to lift a box (65 cm × 35 cm × 15 cm) up to 1-meter height. The load on the box was incremented by 2.25 kg gradually. Once the participant felt that he was uncomfortable with more weight being added, the load was considered as the safe maximum lifting load. Once the maximum weight was determined, the lifting study was initiated. The motion capture data and GRF data were smoothed in Vicon® software using a Butterworth filter with cutoff frequencies of 6 Hz and 25 Hz, respectively.

The subject was requested to lift a box (65 cm × 35 cm × 15 cm) forward for symmetric lifting, in three trials. Because the box did not have handles, it was placed on top of a weight disk about 2.54 cm on the floor so that the subject could fit his fingers under the box. The subject then lifted the box in the most comfortable and natural way and set it down on a 1-m-tall table in front of him, as shown in Fig. 2. After data collection, the motion data post-processing was conducted in the motion capture software Vicon Nexus.

3 Results

The simulation and experimental results are compared in this section. For model simulations, Subject #8 is used. The strength (z_{score}) of the predictive model is 1.05 [23]. For the 3D model, it takes 72.77 s of central processing unit (CPU) time for a desktop computer with an Intel (R) Xeon (R) E-2186G CPU @ 3.80 GHz to solve the nonlinear optimization problem using SNOPT. The predicted maximum lifting weights on the right and left hands are 124.92 N and 120.45 N, respectively; i.e., the total optimal lifting weight is 245.37 N, and the optimal lifting time duration is 1.32 s. For the 2D model, it takes 1.75 s of CPU time to obtain the optimal solution for the same configuration computer and the optimal lifting weight is 220.15 N, and the optimal lifting time duration is 1.439 s. The experimental maximum lifting weight is 233.73 N and the lifting time duration is 1.44 s.

Figure 3 shows the simulated symmetric lifting motions for Subject #8. Figure 4 shows the joint angle comparisons between the simulation and experimental data (Subject #8). Finally, Fig. 5 shows the comparison of GRFs during lifting for Subject #8.

4 Discussion and Conclusions

In this case study, we reported preliminary results of 2D and 3D single-subject symmetric lifting models. Nine important joint angles that play a vital role during symmetric lifting are predicted using the 2D and 3D human models in Fig. 4. There are minor differences between the left and right joint angles for experimental data of Subject #8, although it is a symmetric lifting task. It is noted that the initial, mid-time, and final experimental joint angles of Subject #8 are used as constraints to guide the predicted lifting motion in the optimization formulation. The 3D model can impose those left and right experimental joint angle constraints separately to capture the details of left and right joint angle profiles as shown in Fig. 4. In contrast, the 2D model only has a single arm and leg in the sagittal plane. Therefore, the 2D model uses the average experimental value of the left and right joints to impose joint angle constraints for Subject #8 at initial, mid-time, and final time points. The 3D model captures the pattern of the ankle joint angle profile better than the 2D model. But, in general, both models predict lower body joint angle profiles well. For the upper body joints, the 3D model predicts a more accurate pattern and timing of phase changes than the 2D model, especially for spine flexion. As the box weight is very heavy, the subject needs to transmit a significant amount of force through the elbow joints. The elbow is mainly a hinge joint and the forearm is unsupported. Because of these factors, it is difficult for the subject to maintain stability during the lifting of a heavy weight which results in a jerky elbow motion as shown in Figs. 4(*g*) and 4(*h*). This also makes it difficult for both models to predict the elbow joint angles accurately.

It is interesting to observe that the left and right GRFs are actually quite different for a symmetric lifting task in the experimental results and the 3D model results. There are several reasons for this discrepancy: first, the load on both hands are heavy and high above the center of mass of the subject. Therefore, small initial jerks from the experimental left and right elbow angles can result in big differences on the left and right GRFs. Second, Subject #8 is a righthand dominated person, and the right side joints are taking more loads than the left-side joints. It can be seen from Fig. 5 that the peak value of the right GRF of Subject #8 is larger than that of the left GRF. An important finding from this study is that the predicted kinetics (GRFs) are different between left and

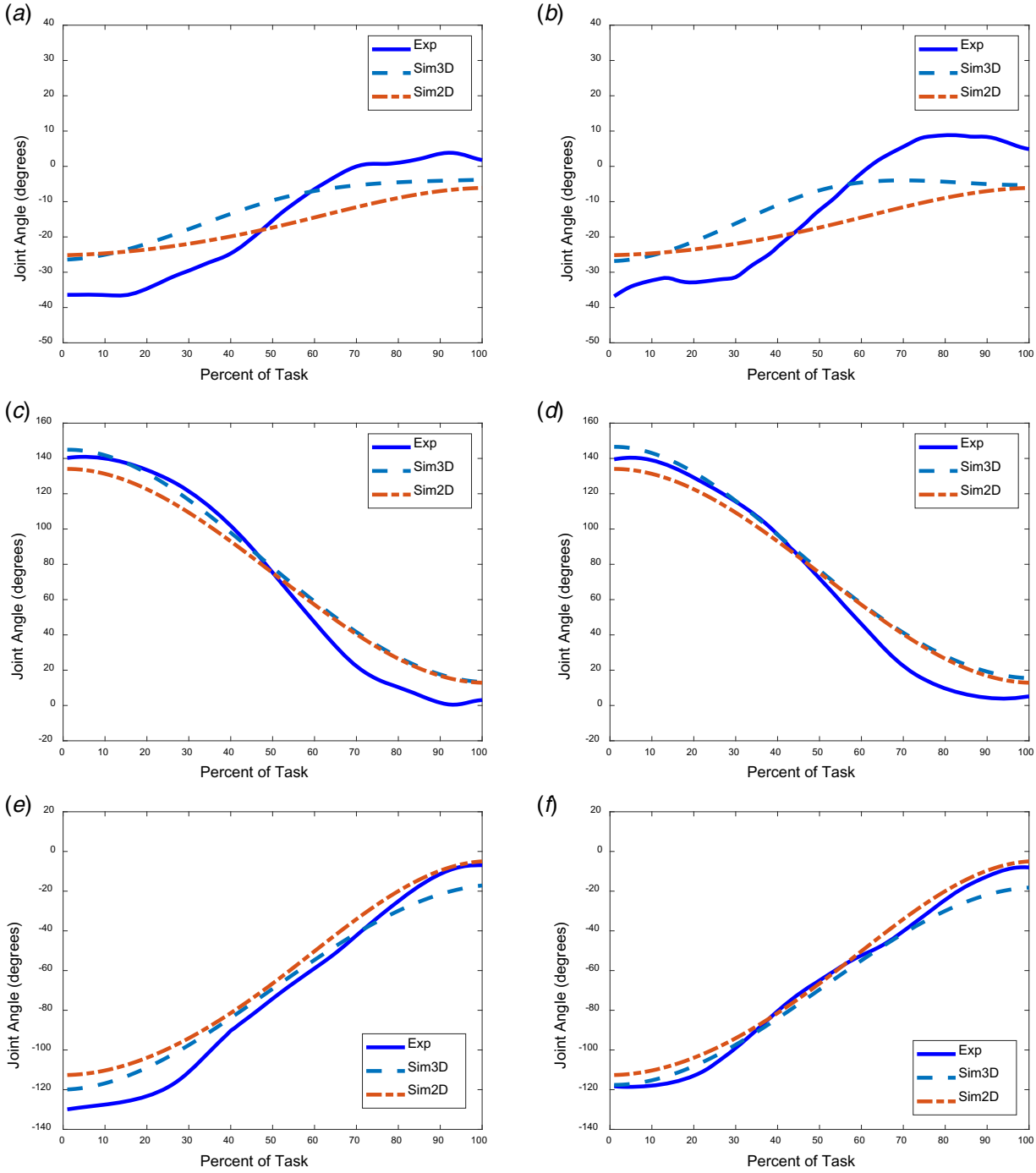

Fig. 4 Joint angle profiles of the symmetric maximum weight lifting: (*a*) left ankle, (*b*) right ankle, (*c*) left knee, (*d*) right knee, (*e*) left hip, (*f*) right hip, (*g*) left elbow, (*h*) right elbow, and (*i*) spine

right feet for a symmetric maximum weight lifting task. The 3D model captures these differences for the individual Subject #8.

The pattern of the predicted right vertical GRF is consistent with the experimental vertical GRF on the right side up to 60% of lifting time using both models as seen in Fig. 5(*b*). In the experimental right GRF profile, there is a trough in the graph from 60 to 90% of the lifting task. That means the GRF is moved from the right side to the left side during that period. As the 2D model does not have the spine, hip, or shoulder rotation, it fails to capture the changes in GRFs as well as the left GRF profile. On the other hand, as the 3D model has rotations for the above-mentioned joints and has the capability to represent the asymmetric GRFs in its kinematics and formulation, it captures the major changes of both GRF profiles. Therefore, the 3D model predicts better trends and magnitudes of both left and right GRFs than the 2D model compared to the experimental data.

Note that 40 N is used as the limits for the GRF constraints in Eqs. (13) and (14) for the 3D model. This limit value is determined based on numerical trial and error considering the convergence capability of the optimizer and robustness of the predictive model. The peak experimental value of GRF of Subject #8 is 660 N, so the relative error for the GRF limit is around 6%. Considering the differences between the mechanical skeletal model and real human model, this relative error for the GRF limit is acceptable.

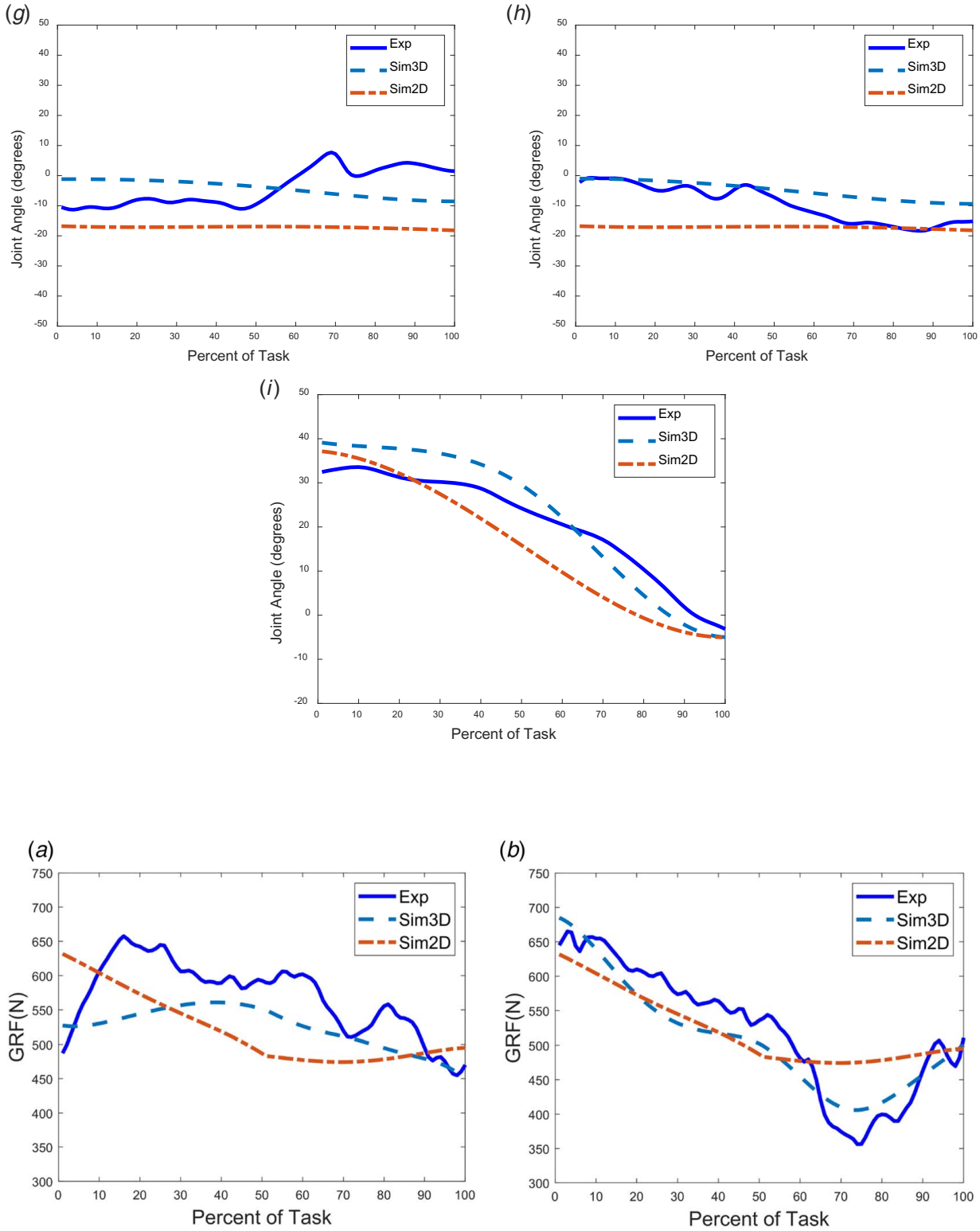

Fig. 5 GRF profiles of the symmetric maximum weight lifting: (*a*) left foot and (*b*) right foot

For the 3D model, the predicted total lifting weight is 245.37 N, which is 5% higher than the experimental lifting weight (233.73 N). The reason is that the maximum lifting weight determined during the experiment is not the true maximum lifting weight. Instead, it is the maximum weight a person felt safe to lift, as mentioned in Sec. 2.4. For the 2D model, the predicted maximum lifting weight is 220.15 N, which is 5.8% lighter than the experimental weight. It demonstrates that the 3D model predicts a more accurate maximum box weight for symmetric lifting.

Figure 3 shows the snapshots of the lifting motion, it is shown that the 3D model has hip adduction during lifting while the 2D model can only generate the motion in the sagittal plane. Another observation is that the 3D model takes more CPU time than the 2D model. This is because the 3D model has more design variables and constraints than the 2D model.

Finally, in this case study, we compared the 2D and 3D optimization formulations for symmetric maximum weight lifting. The two optimization formulations have similar kinds of design variables and objective functions and share some common constraints. The 3D model requires additional constraints to define the lifting task in 3D space. The simulation results are also compared, and preliminary conclusions are drawn below:

(1) 3D symmetric lifting has asymmetric kinetics.
(2) The 2D model is a simplified model and cannot predict asymmetric kinetics of the lifting motion.
(3) The 3D model can predict not only the kinematics difference but also the kinetics difference between the left and right body.
(4) The 2D model is computational more efficient than the 3D model.
(5) For lifting motion prediction, the upper body joints (spine and elbow) are more difficult to predict compared to the lower body joints (hip, knee, and ankle) for both 2D and 3D models.
(6) For lifting motion prediction, it is necessary to incorporate some experimental data in the optimization formulation to predict joint angle profiles and GRFs accurately.
(7) The 3D model is recommended for symmetric maximum weight lifting prediction due to the existence of asymmetric kinetics.

Acknowledgment

This work is supported by the National Science Foundation (CBET: 1849279 and 1703093).

Conflict of Interest

There are no conflicts of interest.

Data Availability Statement

The data sets generated and supporting the findings of this article are obtainable from the corresponding author upon reasonable request.

References

[1] Murray, C. J. L., Lopez, A. D., World Health Organization, and Harvard School of Public Health, 1996, *The Global Burden of Disease: A Comprehensive Assessment of Mortality and Disability From Diseases, Injuries, and Risk Factors in 1990 and Projected to 2020: Summary*, Harvard School of Public Health, Boston, MA.
[2] Freburger, J. K., Holmes, G. M., Agans, R. P., Jackman, A. M., Darter, J. D., Wallace, A. S., Castel, L. D., Kalsbeek, W. D., and Carey, T. S., 2009, "The Rising Prevalence of Chronic Low Back Pain," Archives Int. Med., **169**(3), pp. 251–258.
[3] Pope, M. H., Andersson, G. B., Frymoyer, J. W., and Chaffin, D. B., 1992, *Occupational Low Back Pain: Assessment, Treatment, and Prevention*, CRC Press, Mosby, St. Louis, MO.
[4] Deyo, R. A., and Tsui-Wu, Y. J., 1987, "Descriptive Epidemiology of Low-Back Pain and Its Related Medical Care in the United States," Spine, **12**(3), pp. 264–268.
[5] Deyo, R. A., Cherkin, D., Conrad, D., and Volinn, E., 1991, "Cost, Controversy, Crisis: Low Back Pain and the Health of the Public," Annu. Rev. Public Health, **12**(1), pp. 141–156.
[6] Xiang, Y., Cruz, J., Zaman, R., and Yang, J., 2020, "Multi-Objective Optimization for Two-Dimensional Maximum Weight Lifting Prediction Considering Dynamic Strength," Eng. Opt.
[7] Rakshit, R., Xiang, Y., and Yang, J., 2020, "Dynamic-Joint-Strength-Based Two-Dimensional Symmetric Maximum-Weight Lifting Simulation: Model Development and Validation," J. Eng. Medicine, **234**(7), pp. 660–673.
[8] Zaman, R., Xiang, Y., Cruz, J., and Yang, J., 2020, "Three-Dimensional Asymmetric Maximum Weight Lifting Prediction Considering Dynamic Joint Strength," J. Eng. Med., (under review).
[9] Christophy, M., Senan, N. A. F., Lotz, J. C., and O'Reilly, O. M., 2012, "A Musculoskeletal Model for the Lumbar Spine," Biomech. Model. Mechanobiol., **11**(1/2), pp. 19–34.
[10] Xiang, Y., Arora, J. S., and Abdel-Malek, K., 2012, "3D Human Lifting Motion Prediction With Different Performance Measures," Int. J. Humanoid Rob., **9**(02), p. 1250012.
[11] Xiang, Y., Arora, J. S., Rahmatalla, S., Marler, T., Bhatt, R., and Abdel-Malek, K., 2010, "Human Lifting Simulation Using a Multi-Objective Optimization Approach," Multibody Syst. Dyn., **23**(4), pp. 431–451.
[12] Waters, T. R., and Garg, A., 2010, "Two-Dimensional Biomechanical Model for Estimating Strength of Youth and Adolescents for Manual Material Handling Tasks," Appl. Ergono., **41**(1), pp. 1–7.
[13] Chang, C. C., Brown, D. R., Bloswick, D. S., and Hsiang, S. M., 2001, "Biomechanical Simulation of Manual Lifting Using Spacetime Optimization," J. Biomech., **34**(4), pp. 527–532.
[14] Lin, C. J., Ayoub, M. M., and Bernard, T. M., 1999, "Computer Motion Simulation for Sagittal Plane Lifting Activities," Int. J. Ind. Ergono., **24**(2), pp. 141–155.
[15] Chang, C. C., McGorry, R. W., Lin, J. H., Xu, X., and Hsiang, S. M., 2001, "Prediction Accuracy in Estimating Joint Angle Trajectories Using a Video Posture Coding Method for Sagittal Lifting Tasks," Ergonomics, **53**(8), pp. 1039–1047.
[16] Gündogdu, Ö, Anderson, K. S., and Parnianpour, M., 2005, "Simulation of Manual Materials Handling: Biomechanical Assessment Under Different Lifting Conditions," Technol. Health Care, **13**(1), pp. 57–66.
[17] Hsiang, S. M., and Ayoub, M. M., 1994, "Development of Methodology in Biomechanical Simulation of Manual Lifting," Int. J. Ind. Ergono., **13**(4), pp. 271–288.
[18] Song, J., Qu, X., and Chen, C. H., 2016, "Simulation of Lifting Motions Using a Novel Multi-Objective Optimization Approach," Int. J. Ind. Ergono., **53**, pp. 37–47.
[19] Song, J., Qu, X., and Chen, C. H., 2015, "Lifting Motion Simulation Using a Hybrid Approach," Ergonomics, **58**(9), pp. 1557–1570.
[20] Sreenivasa, M., Millard, M., Kingma, I., Van Dieen, J. H., and Mombaur, K., 2018, "Predicting the Influence of hip and Lumbar Flexibility on Lifting Motions Using Optimal Control," J. Biomech., **78**, pp. 118–125.
[21] Frey-Law, L. A., Laake, A., Avin, K. G., Heitsman, J., Marler, T., and Abdel-Malek, K., 2012, "Knee and Elbow 3D Strength Surfaces: Peak Torque-Angle-Velocity Relationships," J. Appl. Biomech., **28**(6), pp. 726–737.
[22] Hussain, S. J., and Frey-Law, L., 2016, "3D Strength Surfaces for Ankle Plantar-and Dorsi-Flexion in Healthy Adults: An Isometric and Isokinetic Dynamometry Study," J. Foot Ankle Res., **9**(1), p. 43.
[23] Xiang, Y., Zaman, R., Rakshit, R., and Yang, J., 2019, "Subject-Specific Strength Percentile Determination for Two-Dimensional Symmetric Lifting Considering Dynamic Joint Strength," Multibody Syst. Dyn., **46**(1), pp. 63–76.
[24] Xiang, Y., Arora, J. S., and Abdel-Malek, K., 2012, "Hybrid Predictive Dynamics: A New Approach to Simulate Human Motion," Multibody Syst. Dyn., **28**(3), pp. 199–224.
[25] Denavit, J., and Hartenberg, R. S., 1955, "A Kinematic Notation for Lower-Pair Mechanisms Based on Matrices," ASME J. Appl. Mech., **22**, pp. 215–221.
[26] Xiang, Y., Arora, J. S., and Abdel-Malek, K., 2009, "Optimization-Based Motion Prediction of Mechanical Systems: Sensitivity Analysis," Struct. Multidiscip. Optim., **37**(6), pp. 595–608.
[27] Gill, P. E., Murray, W., and Saunders, M. A., 2005, "SNOPT: An SQP Algorithm for Large-Scale Constrained Optimization," SIAM Review, **47**(1), pp. 99–131.